Transcriptional up-regulation of nitric oxide synthase II by nuclear factor-κB at rostral ventrolateral medulla in a rat mevinphos intoxication model of brain stem death

Julie Y. H. Chan[1], Carol H. Y. Wu[2], Ching-Yi Tsai[2], Hsiao-Lei Cheng[2], Kuang-Yu Dai[2], Samuel H. H. Chan[2] and Alice Y. W. Chang[2]

[1]*Department of Medical Education and Research, Kaohsiung Veterans General Hospital, Kaohsiung, Taiwan, Republic of China*
[2]*Center for Neuroscience, National Sun Yat-sen University, Kaohsiung, Taiwan, Republic of China*

As the origin of a 'life-and-death' signal that reflects central cardiovascular regulatory failure during brain stem death, the rostral ventrolateral medulla (RVLM) is a suitable neural substrate for mechanistic delineation of this vital phenomenon. Using a clinically relevant animal model that employed the organophosphate pesticide mevinphos (Mev) as the experimental insult, we evaluated the hypothesis that transcriptional up-regulation of nitric oxide synthase I or II (NOS I or II) gene expression by nuclear factor-κB (NF-κB) on activation of muscarinic receptors in the RVLM underlies brain stem death. In Sprague-Dawley rats maintained under propofol anaesthesia, co-microinjection of muscarinic M2R (methoctramine) or M4R (tropicamide), but not M1R (pirenzepine) or M3R (4-diphenylacetoxy-*N*-dimethylpiperidinium) antagonist significantly reduced the enhanced NOS I–protein kinase G signalling ('pro-life' phase) or augmented NOS II–peroxynitrite cascade ('pro-death' phase) in ventrolateral medulla, blunted the biphasic increase and decrease in baroreceptor reflex-mediated sympathetic vasomotor tone that reflect the transition from life to death, and diminished the elevated DNA binding activity or nucleus-bound translocation of NF-κB in RVLM neurons induced by microinjection of Mev into the bilateral RVLM. However, NF-κB inhibitors (diethyldithiocarbamate or pyrrolidine dithiocarbamate) or double-stranded κB decoy DNA preferentially antagonized the augmented NOS II–peroxynitrite cascade and the associated cardiovascular depression exhibited during the 'pro-death' phase. We conclude that transcriptional up-regulation of NOS II gene expression by activation of NF-κB on selective stimulation of muscarinic M2 or M4 subtype receptors in the RVLM underlies the elicited cardiovascular depression during the 'pro-death' phase in our Mev intoxication model of brain stem death.

(Resubmitted 21 February 2007; accepted after revision 20 March 2007; first published online 29 March 2007)
Corresponding author A. Y. W. Chang: Center for Neuroscience, National Sun Yat-sen University, Kaohsiung 80424, Taiwan, Republic of China. Email: achang@mail.nsysu.edu.tw

An interface between the circulatory system and the central nervous system exists in the brain stem, where fundamental components of central cardiovascular regulation reside (Spyer, 1994). This interface becomes vitally important with the observation that asystole invariably takes place within hours or days after the diagnosis of brain stem death (Pallis, 1983), which implies that permanent impairment of the brain stem cardiovascular regulatory machinery precedes death. Better understanding of the cellular and molecular basis of the interplay between the brain stem regulatory mechanisms and cardiovascular functions should therefore enrich the dearth of information currently available on the mechanisms of brain stem death.

The rostral ventrolateral medulla (RVLM) presents itself as a suitable neural substrate for mechanistic evaluation of brain stem death (JYH Chan *et al.* 2005*b*). In addition to its classical role in tonic maintenance of vasomotor tone in peripheral vasculature (Guertzenstein & Silver, 1974; Ross *et al.* 1984), translational research from our laboratory (see JYH Chan *et al.* 2005*b*) demonstrated that the RVLM is the origin of a 'life-and-death' signal that reflects failure of the central cardiovascular regulatory machinery during brain stem death. Of interest is that the waxing and waning of this 'life-and-death' signal, which mirrors the fluctuation of neuronal activity in the RVLM, manifests itself as the low-frequency component in the systemic arterial pressure (SAP) spectrum (Kuo *et al.* 1997*a*,*b*;

 DOI: 10.1113/jphysiol.2007.130872

Yien *et al.* 1997; Yen *et al.* 2000). Furthermore, the power density of the low-frequency component reflects the prevailing baroreceptor reflex (BRR)-mediated sympathetic vasomotor tone (Li *et al.* 2001).

The RVLM is also a brain stem site via which mevinphos (3-[dimethoxyphosphinyl-oxyl]-2-butenoic acid methyl ester; Mev), a US Environmental Protection Agency Toxicity Category I pesticide, acts to elicit cardiovascular toxicity in our organophosphate intoxication model of brain stem death (JYH Chan *et al.* 2005*b*). As an organophosphate of the P = O type, Mev acts directly in the brain as a cholinesterase inhibitor (Takahashi *et al.* 1991). Our laboratory (Yen *et al.* 2001) demonstrated that activation of muscarinic receptors in the RVLM by accumulated acetylcholine triggers a biphasic increase and decrease in the power density of the low-frequency component of SAP signals, referred to as phase I ('pro-life') and phase II ('pro-death') Mev intoxication. We further established (JYH Chan *et al.* 2004*a*, 2005*a*, 2007) that nitric oxide (NO) generated by NO synthase I (NOS I) in the RVLM, followed by activation of the soluble guanylyl cyclase (sGC)–cGMP–protein kinase G (PKG) cascade, is responsible for the phase I Mev-induced cardiovascular responses. On the other hand, peroxynitrite formed by a reaction between NOS II-derived NO and superoxide anion in the RVLM underlies the subsequent 'pro-death' phase II.

Since death represents the end of existence for an individual, we proposed recently (JYH Chan *et al.* 2005*b*, 2007; Li *et al.* 2005; Chang *et al.* 2006) that multiple 'pro-life' and 'pro-death' regulatory programs must be activated in the RVLM during the progression towards brain stem death. One fertile direction in the search for the cellular and molecular underpinnings of brain stem death is therefore to identify these regulatory programs. Nuclear factor-κB (NF-κB), in this regard, presents itself as a reasonable candidate. NF-κB is one of the transcriptional regulators of the NOS I (Hall *et al.* 1994; CF Chan *et al.* 2000; Jeong *et al.* 2000) and NOS II (Xie *et al.* 1994; Keinanen *et al.* 1999; Wei *et al.* 2004) gene. In addition, this transcription factor is activated on stimulation of seven transmembrane G-protein-coupled receptors such as muscarinic receptors (Todisco *et al.* 1999; Siehler *et al.* 2001).

Based on our Mev intoxication model (JYH Chan *et al.* 2005*b*), the present study evaluated the hypothesis that transcriptional up-regulation of NOS I or II gene expression by NF-κB on activation of muscarinic receptors in the RVLM underlies the transition from the 'pro-life' to the 'pro-death' phase during brain stem death. Our results partially validated this hypothesis. We observed that whereas stimulation of muscarinic M2 or M4 subtype receptors in the RVLM underlies both phases of Mev intoxication and the associated NOS I–PKG or NOS II–peroxynitrite signalling cascades, this muscarinic activation of NF-κB is preferentially involved in the elicited cardiovascular depression during the 'pro-death' phase via transcriptional up-regulation of NOS II gene expression in the RVLM.

Methods

Adult male Sprague–Dawley rats (295–358 g, $n = 277$) purchased from the Experimental Animal Center of the National Science Council, Taiwan, Republic of China were used. All experimental procedures were carried out in compliance with the guidelines of our institutional animal care committee.

General preparation

Preparatory surgery was carried out under an induction dose of pentobarbital sodium (50 mg kg^{-1}, I.P.), and included cannulation of a femoral artery and both femoral veins, together with tracheal intubation. During the recording session, which routinely commenced 60 min after the administration of pentobarbital sodium, anaesthesia was maintained by intravenous infusion of propofol (Zeneca, Macclesfield, UK) at 20–25 mg kg^{-1} h^{-1}. We have demonstrated (Yang *et al.* 1995) that this scheme provided satisfactory anaesthetic maintenance while preserving the capacity of central circulatory regulation. During the recording session, body temperature of the animals was maintained at 37°C with a heating pad, and animals were allowed to breathe spontaneously with room air.

Mev intoxication model of brain stem death

The Mev intoxication model of brain stem death (JYH Chan *et al.* 2005*b*) was used. Since systemically administered Mev acts on the RVLM to elicit comparable cardiovascular responses (Yen *et al.* 2001), direct application of Mev to this brain stem site has been routinely carried out (Yen *et al.* 2001; JYH Chan *et al.* 2004*a*, 2005*a*, 2007) to produce site-specific actions. SAP signals recorded from the femoral artery were simultaneously subjected to on-line power spectral analysis (SHH Chan *et al*. 2001, 2005; JYH Chan *et al.* 2004*a*,*b*, 2005*a*, 2007; Li *et al.* 2005; Chang *et al.* 2006). We were particularly interested in the low-frequency (0.25–0.8 Hz) component in the SAP spectrum because its power density mirrors the prevalence of BBR-mediated sympathetic neurogenic vasomotor discharges that emanate from this brain stem site (Li *et al.* 2001). More importantly, our laboratory demonstrated previously (JYH Chan *et al.* 2004*a*, 2005*a*, 2007) that the power density of this spectral signal exhibits biphasic changes that reflect the 'pro-life' and 'pro-death' phases seen during the progression towards brain stem

death in patients who succumbed to organophosphate poisoning (Yen *et al.* 2000). Heart rate (HR) was derived instantaneously from SAP signals. Temporal changes in the power density of the low-frequency component, pulsatile SAP, mean SAP (MSAP) and HR were routinely followed for 180 min in an on-line and real-time manner.

Microinjection of test agents

Microinjection bilaterally of test agents into the RVLM, each at a volume of 50 nl, was carried out stereotaxically and sequentially as detailed in previous studies (Yen *et al.* 2001; JYH Chan *et al.* 2004*a*,*b*, 2005*a*, 2007; SHH Chan *et al*. 2005; Li *et al.* 2005; Chang *et al.* 2006). The coordinates used were: 4.5–5 mm posterior to lambda, 1.8–2.1 mm lateral to midline, and 8.1–8.4 mm below the dorsal surface of cerebellum. These coordinates were selected to cover the ventrolateral medulla at which functionally identified sympathetic premotor neurons reside (Ross *et al.* 1984). As shown recently (JYH Chan *et al.* 2007), microinjected test agents exhibited a discrete diffusion of approximately 800 μm × 800 μm to an area in the medulla oblongata (see Fig. 6*A*) that is below the nucleus ambiguus, lateral to the inferior olivary nucleus and medial to the spinal trigeminal nucleus (Paxinos & Watson, 2007). Test agents used included Mev (kindly provided by Huikwang Corporation, Tainan, Taiwan), selective muscarinic M1R antagonist (Hagan *et al.* 1987), pirenzepine (Sigma-Aldrich, St Louis, MO, USA); selective M2R antagonist (Giraldo *et al.* 1988), methoctramine (Sigma-Aldrich); selective M3R antagonist (Waelbroeck *et al.* 1992), 4-diphenylacetoxy-*N*-dimethylpiperidinium (4-DAMP; Tocris Cookson, Bristol, UK); selective M4R antagonist (Liu & Lee, 1999), tropicamide (Tocris Cookson); selective NF-κB inhibitors (Schreck *et al.* 1992; Hill *et al.* 2001), sodium diethyldithiocarbamate (DDTC; Sigma-Aldrich) or pyrrolidine dithiocarbamate (PDTC; Sigma-Aldrich); or double-stranded κB decoy DNA (5′-GAGGGGACTTTCCCT-3′ and 3′-CTCCC-CTGAAAGGGA-5′) or its scrambled sequence (5′-GAT-GCGTCTGTCGCA-3′ and 3′-CTACGCAGACAGCGT-5′) (Yeh *et al.* 2002; JYH Chan *et al.* 2004*b*; Quality Systems, Taipei, Taiwan). With the exception of double-stranded κB decoy DNA or its scrambled sequence, which was microinjected bilaterally into the RVLM 24 h before the administration of Mev, all other test agents were given together with Mev in a single injection (JYH Chan *et al.* 2004*a*, 2005*a*, 2007). The doses were adopted from previous reports (Hagan *et al.* 1987; Giraldo *et al.* 1988; Schreck *et al.* 1992; Waelbroeck *et al.* 1992; Liu & Lee, 1999; Hill *et al.* 2001; JYH Chan *et al.* 2004*a*,*b*, 2005*a*, 2007) that used those test agents for the same purpose as in this study. Microinjection of artificial cerebrospinal fluid (aCSF) or individual solvents served as the vehicle control. The composition of aCSF was (mM): NaCl 117, $NaHCO_3$ 25, glucose 11, KCl 4.7, $CaCl_2$ 2.5, $MgCl_2$ 1.2 and NaH_2PO_4 1.2. To avoid the confounding effects of drug interactions, each animal received only one pharmacological treatment. As a routine, results from five to six animals that received the same treatment constituted an experimental group.

Collection of tissue samples from ventrolateral medulla

Since the power density of the low-frequency component in the SAP spectrum reflects the prevalence of the 'life-and-death' signal detected from patients intoxicated with organophosphate poisons (Yen *et al.* 2000), we routinely collected tissue samples for subsequent biochemical evaluations (JYH Chan *et al.* 2004*a*, 2005*a*, 2007; SHH Chan *et al*. 2005) during the peak of the 'pro-life' and 'pro-death' phase (Mev group), or 30 or 180 min after microinjection of aCSF into the RVLM (vehicle control). Animals were killed with an overdose of pentobarbital sodium and tissues from both sides of the ventrolateral medulla, at the level of the RVLM (0.5–1.5 mm rostral to the obex), were collected by micro-punches made with a 1 mm (i.d.) stainless-steel bore to cover the anatomical boundaries of the RVLM (see Fig. 6*A*) that were co-extensive with the distribution of the micro-injected test agents (JYH Chan *et al.* 2007). Medullary tissues collected from anaesthetized animals but without treatment served as the sham-controls. The concentration of total proteins extracted from those tissue samples was determined by the BCA protein assay (Pierce, Rockford, IL, USA). In some experiments, proteins from the nuclear or cytosolic fraction of the medullary samples were extracted by a commercial kit (Active Motif, Carlsbad, CA, USA), and their concentrations similarly quantified.

Western blot analysis

Western blot analysis (Chang *et al.* 2003, 2006; JYH Chan *et al.* 2004*a*,*b*, 2005*a*, 2007; SHH Chan *et al*. 2005; Li *et al.* 2005) was carried out using a rabbit polyclonal antiserum against NOS I, NOS II, NOS III (Santa Cruz, Santa Cruz, CA, USA) or PKG (Calbiochem, San Diego, CA, USA); or a mouse monoclonal antiserum against nitrotyrosine (Upstate, Lake Placid, NY, USA) or β-actin (Chemicon, Temecula, CA, USA). This was followed by incubation with horseradish peroxidase-conjugated donkey anti-rabbit IgG (Amersham Biosciences, Little Chalfont, Bucks, UK) for NOS I, II or III or PKG, or sheep anti-mouse IgG (Amersham Biosciences) for nitrotyrosine or β-actin. Specific antibody–antigen complex was detected by an enhanced chemiluminescence Western blot detection system (NEN, Boston, MA, USA). The amount of protein product was quantified by the ImageMaster Video Documentation System (Amersham Pharmacia Biotech), and was expressed as the ratio to β-actin protein.

Electrophoresis mobility shift assay

We employed the electrophoresis mobility shift assay (EMSA) (Yeh *et al.* 2002; JYH Chan *et al.* 2004*b*) to measure NF-κB DNA binding activity in nuclear proteins extracted from ventrolateral medulla. The 3′ end of a double-stranded synthetic oligonucleotide probe for NF-κB (5′-AGTGAGGGGACTTTCCCAGGC-3′ and 3′-TCAACTCCCCTGAAAGGGTCCG-5′) (Yeh *et al.* 2002; JYH Chan *et al.* 2004*b*) was labelled with digoxigenin-11-ddUTP (Roche, Penzberg, Germany). DNA and protein complexes resolved on 4% polyacrylamide gels by electrophoresis were detected by chemiluminescence after reacting with an anti-digoxigenin antiserum. A rabbit polyclonal antiserum against NF-κB p50, p65 or c-Rel subunit (Santa Cruz) was added to the DNA binding reaction cocktail in supershift assay to determine the participation of NF-κB subunits. Competitive assay using unlabelled NF-κB oligonucleotide served as the negative control. We further employed Western blot analysis to detect the NF-κB p50 or p65 subunit in the nuclear or cytosolic fraction of extracts from ventrolateral medulla (JYH Chan *et al.* 2004*b*).

Double immunofluorescence staining and laser confocal microscopy

Double immunofluorescence staining (Chang *et al.* 2003, 2006; JYH Chan *et al.* 2004*a*, 2007; SHH Chan *et al*. 2005) was carried out using a rabbit polyclonal antiserum against NF-κB p65 subunit (Santa Cruz) and a mouse monoclonal antiserum against a specific neuronal marker (Chang *et al.* 2003, 2006; JYH Chan *et al.* 2007), neuron-specific nuclear protein (NeuN; Chemicon). The secondary antisera included a goat anti-rabbit IgG conjugated with Alexa Fluor 488 and a goat anti-mouse IgG conjugated with Alexa Fluor 568 (Molecular Probes, Eugene, OR, USA). Tissues similarly processed but omitting anti-NF-κB p65 subunit antiserum served as our negative control. Viewed under a Fluorview FV300 laser scanning confocal microscope (Olympus, Tokyo, Japan), immunoreactivity for NeuN exhibited red fluorescence and NF-κB manifested green fluorescence. The exhibition of yellow fluorescence on clearly defined nucleus and nucleolus in RVLM neurons was indicative of a shift of NF-κB immunoreactivity from the cytoplasm to the nucleus.

Histology

In some animals that were not used for biochemical analysis, the brain stem was removed at the end of the physiological experiment and fixed in 30% sucrose in 10% formaldehyde–saline solution for at least 72 h. Frozen 25 μm sections of the medulla oblongata stained with neural red were used for histological verification of the microinjection sites.

Statistical analysis

All values are expressed as mean ± S.E.M. The averaged value of MSAP or HR calculated every 20 min after administration of test agents or vehicle, the sum total of power density for the low-frequency component in the SAP spectra over 20 min, or the protein expression level in the ventrolateral medulla during each phase of Mev intoxication, were used for statistical analysis. One-way or two-way ANOVA with repeated measures was used, as appropriate, to assess group means. This was followed by the Scheffé multiple-range test for *post hoc* assessment of individual means. $P < 0.05$ was considered to be statistically significant.

Results

Mev elicits biphasic cardiovascular responses via selective activation of muscarinic M2R or M4R in RVLM

Our first series of experiments established a causal relationship between individual muscarinic subtype receptors in the RVLM and Mev-induced biphasic cardiovascular responses. As reported previously (JYH Chan *et al.* 2004*a*, 2005*a*, 2007), co-microinjection bilaterally of Mev (10 nmol) and aCSF or a relevant vehicle into the RVLM resulted in a progressive decline in MSAP that became significant 100 min after application (Fig. 1), accompanied by an indiscernible change in HR. Concurrent changes in power density of the low-frequency component of SAP signals revealed two distinct phases. Phase I entailed a significantly augmented low-frequency power that endured 100 min. Phase II, which lasted the remainder of our 180 min observation period, exhibited further and significant reduction in the power density of this spectral component to below baseline.

In the presence of a selective muscarinic M2R antagonist, methoctramine (0.5 or 1 nmol), or a selective muscarinic M4R antagonist, tropicamide (0.5 or 1 nmol), the hypotension promoted by Mev was significantly and dose-dependently blunted. Likewise, both the augmented power density of the low-frequency component of SAP signals during phase I Mev intoxication and the reduced low-frequency power during phase II were significantly antagonized (Fig. 1). On the other hand, co-administration of a selective muscarinic M1R antagonist, pirenzepine (0.5 or 1 nmol), or a selective muscarinic M3R antagonist, 4-DAMP (0.5 or 1 nmol), was ineffective.

Selective activation of muscarinic M2R or M4R in RVLM underlies Mev-induced phasic augmentation of NOS I, PKG, NOS II or nitrotyrosine expression in ventrolateral medulla

We next evaluated whether a causal relationship exists between muscarinic M2R or M4R in the RVLM and Mev-induced phasic changes in the NOS I–PKG or NOS II–peroxynitrite signalling cascade. Also similar to previous observations (JYH Chan *et al.* 2004*a*, 2005*a*, 2007), Western blot analysis (Fig. 2) revealed that NOS I or PKG expression in ventrolateral medulla manifested a significant surge during phase I, followed by a return to baseline during phase II. On the other hand, the level of NOS II or nitrotyrosine, an experimental marker for peroxynitrite (JYH Chan *et al.* 2005*a*, 2007; Li *et al.* 2005), was progressively and significantly augmented over both phases. Interestingly, whereas those Mev-induced phasic changes in NOS I, PKG, NOS II or nitrotyrosine were significantly antagonized on co-microinjection of methoctramine or tropicamide into the bilateral RVLM, pirenzepine or 4-DAMP was ineffective. NOS III expression in the ventrolateral medulla remained essentially unaltered during both phases of Mev intoxication (Fig. 2), and was not affected by the muscarinic receptor antagonists.

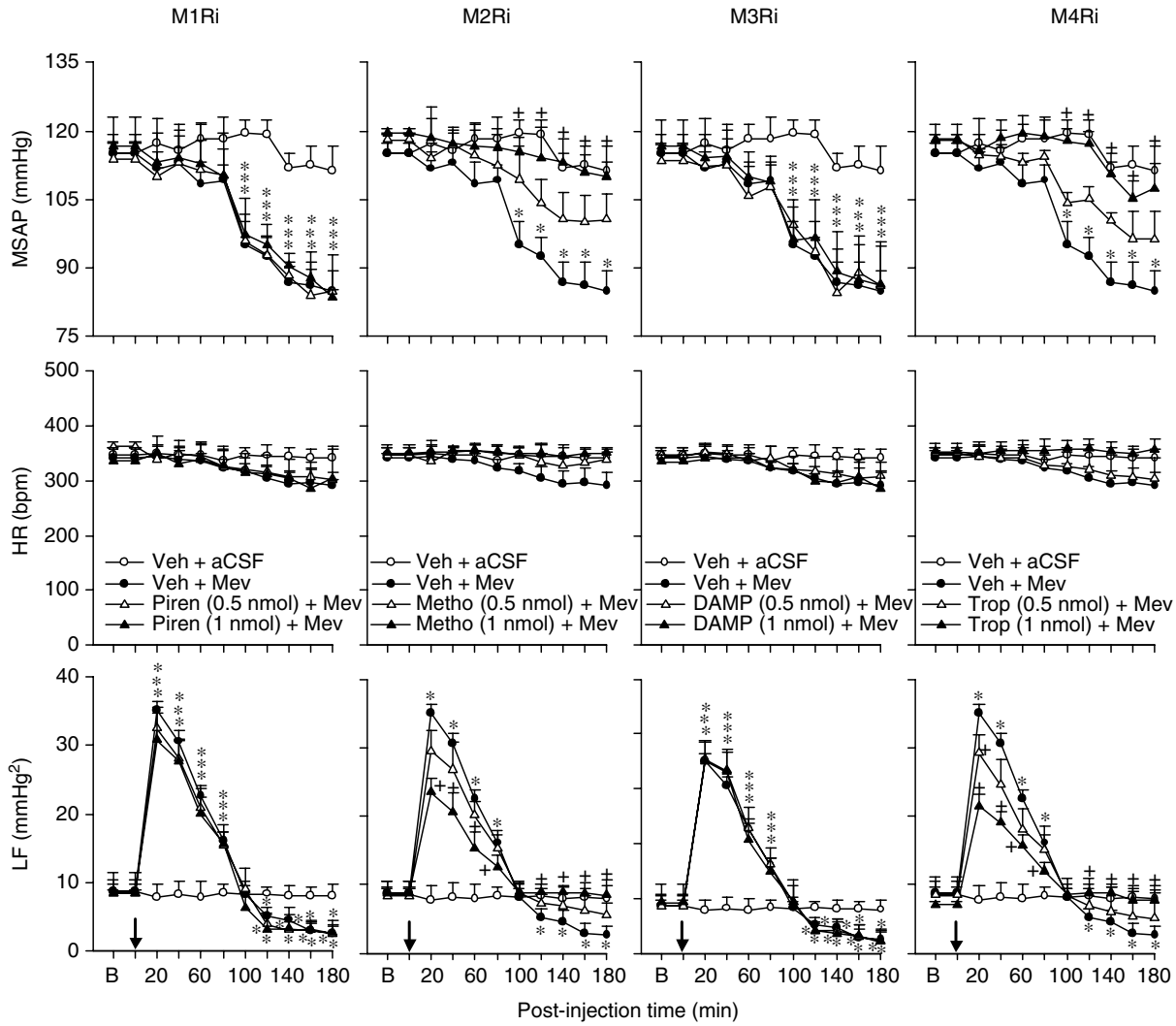

Figure 1. Effects of selective blockade of muscarinic receptor subtypes in RVLM on cardiovascular responses during Mev intoxication

Temporal changes in mean systemic arterial pressure (MSAP), heart rate (HR) or power density of low-frequency (LF) component of SAP spectrum in animals that received microinjection bilaterally into the RVLM (at arrow) of Mev (10 nmol) or aCSF, given together with individual muscarinic receptor antagonists (M1Ri to M4Ri) or their solvent (Veh). Values are mean ± S.E.M., $n = 5$–6 animals per experimental group. $^{*}P < 0.05$ *vs.* Veh + aCSF group and $^{+}P < 0.05$ *vs.* Veh + Mev group at corresponding time-points in the Scheffé's multiple-range analysis.

Activation of NF-κB in RVLM selectively underlies Mev-induced cardiovascular depression

Our third series of experiments further established a causal relationship between Mev-induced activation of NF-κB in the RVLM and biphasic cardiovascular responses, using loss-of-function manipulations that included pharmacological blockade and gene knockdown. Figure 3 showed that the significant hypotension induced by Mev (100 nmol) during phase II was blunted in the presence

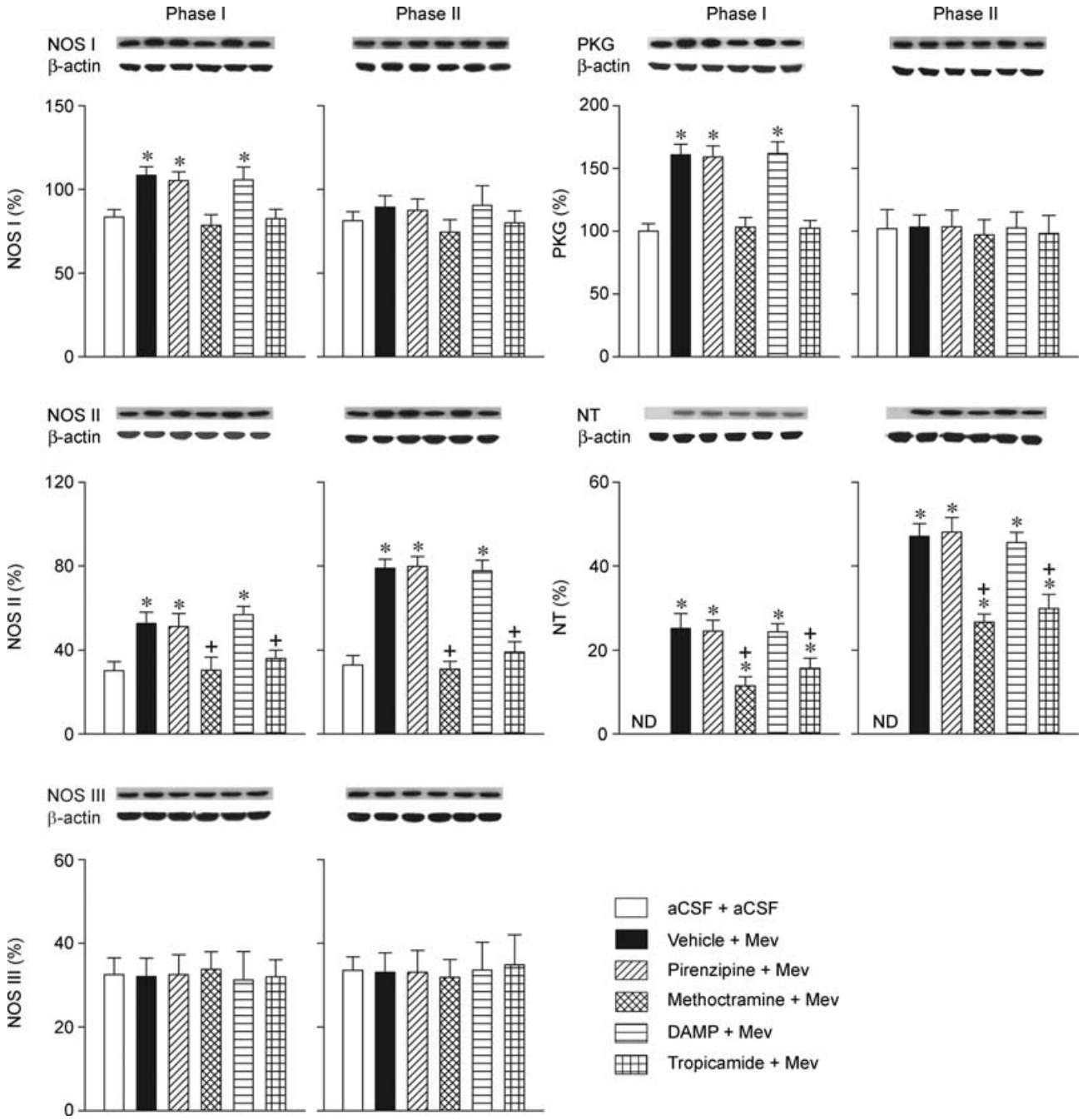

Figure 2. Effects of selective blockade of muscarinic receptor subtypes in RVLM on NOS I–PKG or NOS II–peroxynitrite signalling cascade in ventrolateral medulla during Mev intoxication
Representative Western blots (insets), or percentage of NOS I, II or III, PKG or nitrotyrosine (NT) relative to β-actin protein, detected from the ventrolateral medulla 30 min (Phase I) or 180 min (Phase II) after animals received bilateral microinjection into RVLM of Mev (10 nmol) or aCSF, given together with individual muscarinic receptor antagonists or their solvent (Vehicle). Values are mean ± S.E.M. of triplicate analyses, $n = 5$–6 animals per experimental group. $^{*}P < 0.05$ *vs.* aCSF + aCSF group, and $^{+}P < 0.05$ *vs.* Vehicle + Mev group in the Scheffé's multiple-range analysis. ND, below detection limit.

of two selective NF-κB inhibitors, DDTC (75 nmol) or PDTC (75 nmol). Likewise, the augmented power density of the low-frequency component during phase I Mev intoxication was enhanced, and the reduced low-frequency power during phase II was significantly antagonized. Bilateral microinjection of double-stranded κB decoy DNA (100 pmol), 24 h prior to Mev treatment essentially duplicated those results (Fig. 3), although pre-treatment with double-stranded DNA with a scrambled sequence was ineffective.

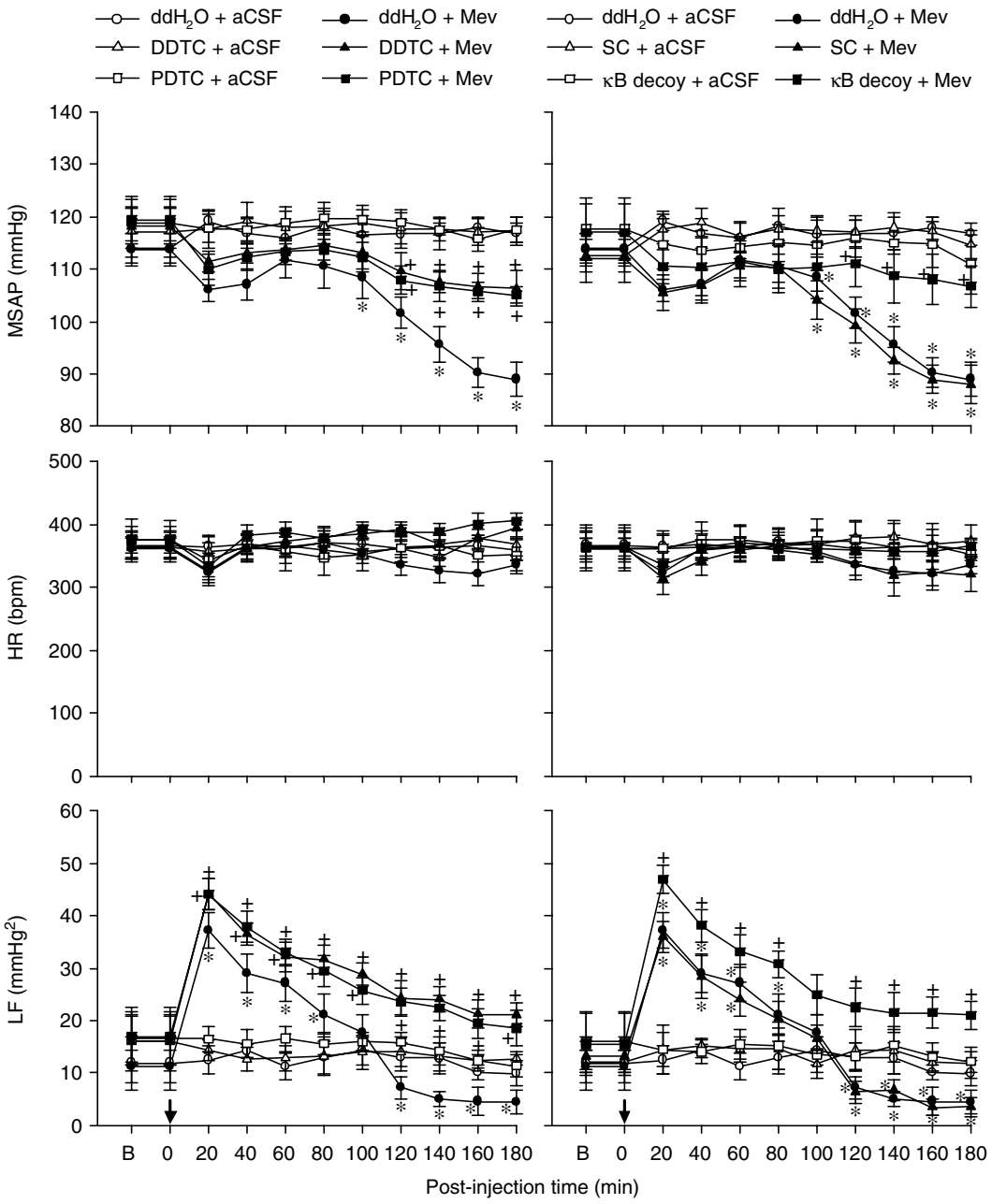

Figure 3. Effects of loss-of-function manipulations of NF-κB in RVLM on cardiovascular responses during Mev intoxication

Temporal changes in MSAP, HR or power density of LF component of SAP spectrum in animals that received microinjection bilaterally into the RVLM (at arrow) of Mev (10 nmol) or aCSF, given together with NF-κB inhibitors DDTC or PDTC (75 nmol) or their solvent, double distilled water (ddH_2O) (left panels); or 24 h after animals received microinjection into the bilateral RVLM of double-stranded κB decoy or scrambled (SC) DNA (100 pmol) (right panels). Values are mean ± S.E.M., $n = 5$–6 animals per experimental group. $^*P < 0.05$ *vs*. ddH_2O + aCSF group and $^+P < 0.05$ *vs*. ddH_2O + Mev group at corresponding time points in the Scheffé's multiple-range analysis.

Selective activation of muscarinic M2R or M4R in RVLM underlies Mev-induced nucleus-bound translocation of NF-κB in ventrolateral medulla

Results from EMSA (Fig. 4*A*) demonstrated a significant and progressive increase in the association of NF-κB with its consensus DNA oligonucleotide in nuclear extracts from the ventrolateral medulla during both phases of Mev intoxication. We confirmed that this association was not due to non-specific binding when a competitive assay using unlabelled NF-κB oligonucleotide resulted in discernible disappearance of NF-κB DNA binding (Fig. 4*B*). Supershift experiments (Fig. 4*B*) further revealed that the major NF-κB subunit activated

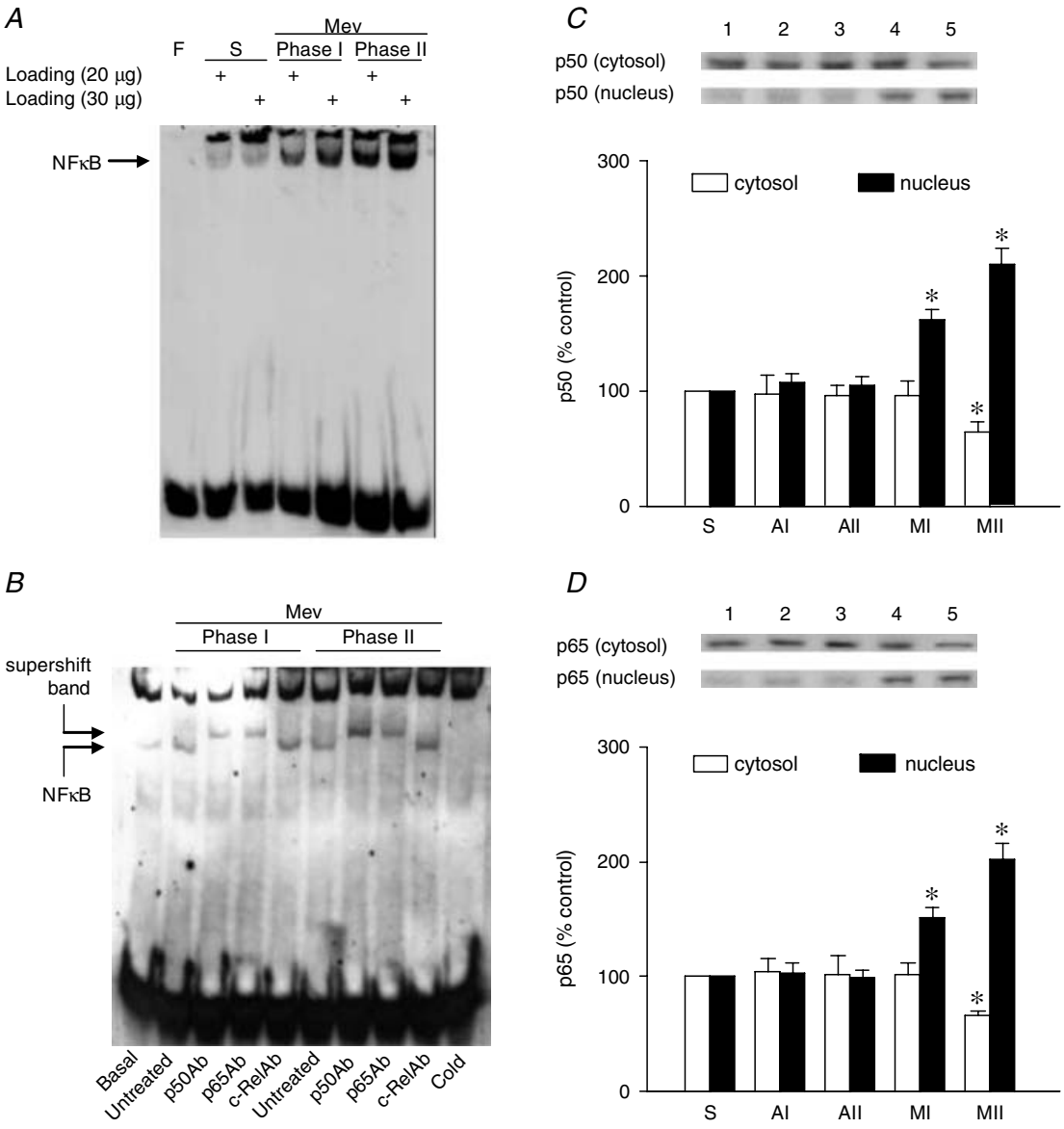

Figure 4. EMSA and Western blot analysis of nucleus-bound translocation of NF-κB in ventrolateral medulla during Mev intoxication

A, representative gel depicting NF-κB DNA binding in nuclear extracts from the ventrolateral medulla of sham-controls (S or Basal), or during Phases I or II cardiovascular responses to Mev (10 nmol). Note that two sample-loading volumes were used to validate our results. F, free probe. *B*, NF-κB DNA binding in nuclear extracts from the ventrolateral medulla pre-incubated in the absence (untreated) or presence of antiserum against p50, p65 or c-Rel subunit of NF-κB. A competitive assay with the addition of 100-fold unlabelled NF-κB oligonucleotide was used to control for non-specific binding (Cold). *C* and *D*, temporal changes as percentage relative to sham-controls (S) of cytosolic and nuclear content of NF-κB p50 or p65 subunit in the ventrolateral medulla of animals 30 min (AI or MI) or 180 min (AII or MII) after animals received bilateral microinjection into RVLM of aCSF or Mev (10 nmol). Values are mean ± S.E.M. of triplicate analyses on samples pooled from 5 to 6 animals in each group. $^*P < 0.05$ *vs.* sham-control or corresponding aCSF group in the Scheffé's multiple-range analysis.

was the p65–p50 heterodimer, as p65 or p50, but not c-Rel, antiserum retarded the migration of proteins that interacted with the double-stranded NF-κB oligonucleotide. That the implicated nucleus-bound translocation of NF-κB indeed took place was confirmed when immunoblot analysis revealed a significant decline of p50 (Fig. 4*C*) or p65 (Fig. 4*D*) subunit of NF-κB protein in the cytosolic fraction, alongside a progressive elevation in the nuclear fraction during Mev intoxication. Intriguingly, all those manifestations of augmented nuclear NF-κB DNA binding activity (Fig. 5) during Mev intoxication were antagonized by methoctramine or tropicamide. Co-microinjection bilaterally of pirenzepine or 4-DAMP into the RVLM, however, was ineffective.

To confirm that the nucleus-bound translocation of NF-κB demonstrated in our biochemical analyses on protein extracts from ventrolateral medulla indeed took place at the neuronal level, our fifth series of experiments examined the intracellular expression of NF-κB in the RVLM (Fig. 6*A*) during Mev intoxication using double immunofluorescence staining. Viewed under a laser scanning confocal microscope, NF-κB was absent from RVLM cells that were immunoreactive to the neuronal marker NeuN (Chang *et al.* 2003, 2006; JYH Chan *et al.* 2007) in negative control experiments (Fig. 6*B*). On the other hand, against a clearly defined nucleus and nucleolus, immunoreactivity for NF-κB was present in the cytoplasm of NeuN-positive cells in sham-control animals (Fig. 6*C*). On microinjection of Mev bilaterally into the RVLM (Fig. 6*C*), there was a progressive shift of NF-κB immunoreactivity from the cytoplasm to the nucleus. Intriguingly, this exhibition of nucleus-bound translocation of NF-κB in RVLM neurons during Mev intoxication was antagonized by methoctramine or tropicamide, but not by pirenzepine or 4-DAMP (Fig. 6*C*). We also noted the presence of residual NF-κB immunoreactivity in our preparations, although it was not double-labelled with NeuN (Fig. 6*C*).

Activation of NF-κB in RVLM preferentially underlies Mev-induced augmentation of NOS II or nitrotyrosine in ventrolateral medulla

In our sixth series of experiments, microinjection of double-stranded κB decoy DNA (100 pmol) bilaterally into the RVLM significantly antagonized the augmented NOS II or nitrotyrosine expression induced by Mev in ventrolateral medulla (Fig. 7). Intriguingly, the augmented NOS I or PKG expression during phase I was not affected. Double-stranded DNA with a scrambled sequence was also ineffective against Mev-induced phasic changes in NOS I, PKG, NOS II or nitrotyrosine.

Microinjection sites

Random histological verifications indicated that all muscarinic receptor antagonists, NF-κB inhibitors, double-stranded κB decoy DNA or its scrambled sequence were delivered bilaterally to the RVLM. Microinjection of test agents into areas adjacent to the anatomical confines of the RVLM elicited minimal effect on our physiological, biochemical or morphological indices.

Discussion

Based on a clinically relevant experimental model of brain stem death (Yen *et al.* 2000; JYH Chan *et al.* 2005*b*), the present study provided novel demonstrations that selective activation of muscarinic M2R or M4R in the RVLM elicited both 'pro-life' and 'pro-death' phases of cardiovascular responses during Mev intoxication, along with activation of the NF-κB and NOS I–PKG or NOS II–peroxynitrite signalling cascade in ventrolateral medulla. We further unveiled that this muscarinic activation of NF-κB, however, is involved preferentially in evoking cardiovascular depression during the 'pro-death' phase via transcriptional up-regulation of NOS II gene expression in the RVLM.

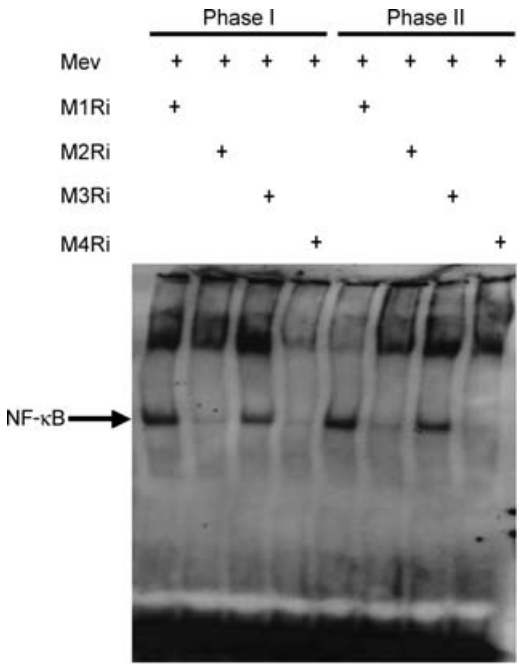

Figure 5. Effects of selective blockade of muscarinic receptor subtypes in RVLM on EMSA analysis of nucleus-bound translocation of NF-κB in ventrolateral medulla during Mev intoxication
Representative gel depicting NF-κB DNA binding in nuclear extracts from the ventrolateral medulla 30 min (Phase I) or 180 min (Phase II) after animals received bilateral microinjection into RVLM of Mev (10 nmol), given alone or together with individual muscarinic receptor antagonists (M1Ri to M4Ri).

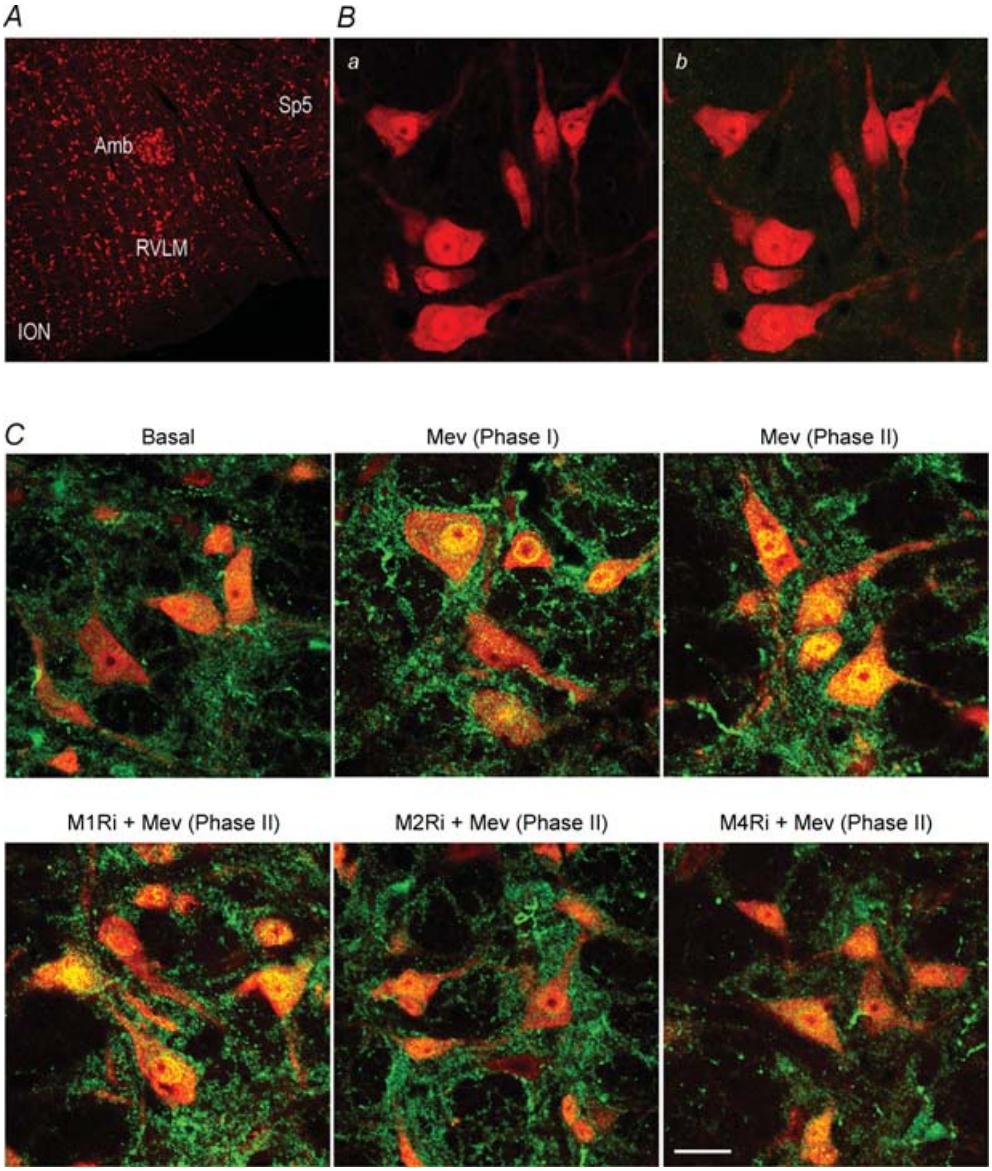

Figure 6. Effects of selective blockade of muscarinic receptor subtypes in RVLM on nucleus-bound translocation of NF-κB in RVLM neurons during Mev intoxication

A, low-power laser scanning confocal microscopic image showing the location of RVLM where high-power photomicrographs of cells that were immunoreactive to a neuronal marker, NeuN (red fluorescence) were obtained. Also shown are anatomical landmarks adjacent to the RVLM in the medulla oblongata. *B*, representative photomicrographs showing NeuN-immunoreactive cells in the RVLM (a) that stained negatively for NF-κB p65 subunit (b) in control experiments when antiserum against this NF-κB subunit was omitted during immunofluorescence processing. *C*, representative confocal microscopic images showing cells in the RVLM that were immunoreactive to NeuN and additionally stained positively for NF-κB p65 subunit in sham-controls (Basal); or during phases I or II cardiovascular responses to Mev, given alone or together with individual muscarinic receptor antagonists. Note in sham-control animals, NF-κB immunoreactivity (green fluorescence) was present in the cytoplasm of NeuN-positive cells (red fluorescence) against clearly defined nucleus and nucleolus. In Mev-treated animals, there was a progressive increase in yellow fluorescence (red plus green fluorescence) in the nucleus of RVLM neurons of Mev-treated animals indicative of a nucleus-bound translocation of NF-κB immunoreactivity from the cytoplasm; and its blockade by M2Ri or M4Ri. Since the residual NF-κB immunoreactivity in the background was not double-labelled with NeuN, it is unlikely to be of neuronal origin. These results are typical of 5 animals from each experimental group. Scale bar, 250 μm in *A* and 20 μm in *B* and *C*. Amb, nucleus ambiguus; ION, inferior olivary nucleus; RVLM, rostral ventrolateral medulla; Sp5, spinal trigeminal nucleus.

Selective activation of muscarinic M2R or M4R in RVLM underlies both phases of cardiovascular responses during Mev intoxication

Our results showed that selective activation of muscarinic M2R or M4R in the RVLM by Mev leads to both phases of cardiovascular responses. Cholinergic terminals synapse with RVLM neurons (Milner *et al.* 1990), and biosynthetic enzymes for (Palkovits & Jacobowitz, 1974; Kobayashi *et al.* 1975; Arneric *et al.* 1990), and releasable pools of (Ernsberger *et al.* 1988), acetylcholine are present in this medullary site. Of the two major subtypes of cholinergic receptors, it is generally contended that the muscarinic receptors in the RVLM play a more prominent role than the nicotinic subtype in cardiovascular regulation. The RVLM is one of the brain substrates with the highest muscarinic receptor binding density (Kellar *et al.* 1985; Arneric *et al.* 1990), and acetylcholine acts preferentially through muscarinic receptors in this medullary region (Willette *et al.* 1984; Li *et al.* 1995) to elicit cardiovascular actions (Willette *et al.* 1984; Kubo *et al.* 1997) or neuronal responses (Huangfu *et al.* 1997). Thus, it is conceivable that, while similarly acting on muscarinic M2R or M4R, the progressively accumulated acetylcholine in the RVLM because of Mev-induced cholinesterase inhibition is responsible for our observed shift from an augmented power density of the low-frequency component of SAP signals during the 'pro-life' phase to a reduction of low-frequency power during the 'pro-death' phase.

Selective activation of muscarinic M2R or M4R in RVLM underlies both NOS I–PKG and NOS II–peroxynitrite signalling cascades in ventrolateral medulla during Mev intoxication

We further showed that the key to the biphasic cardiovascular event after selective activation of muscarinic M2R or M4R is NO generated, respectively, by NOS I or NOS II

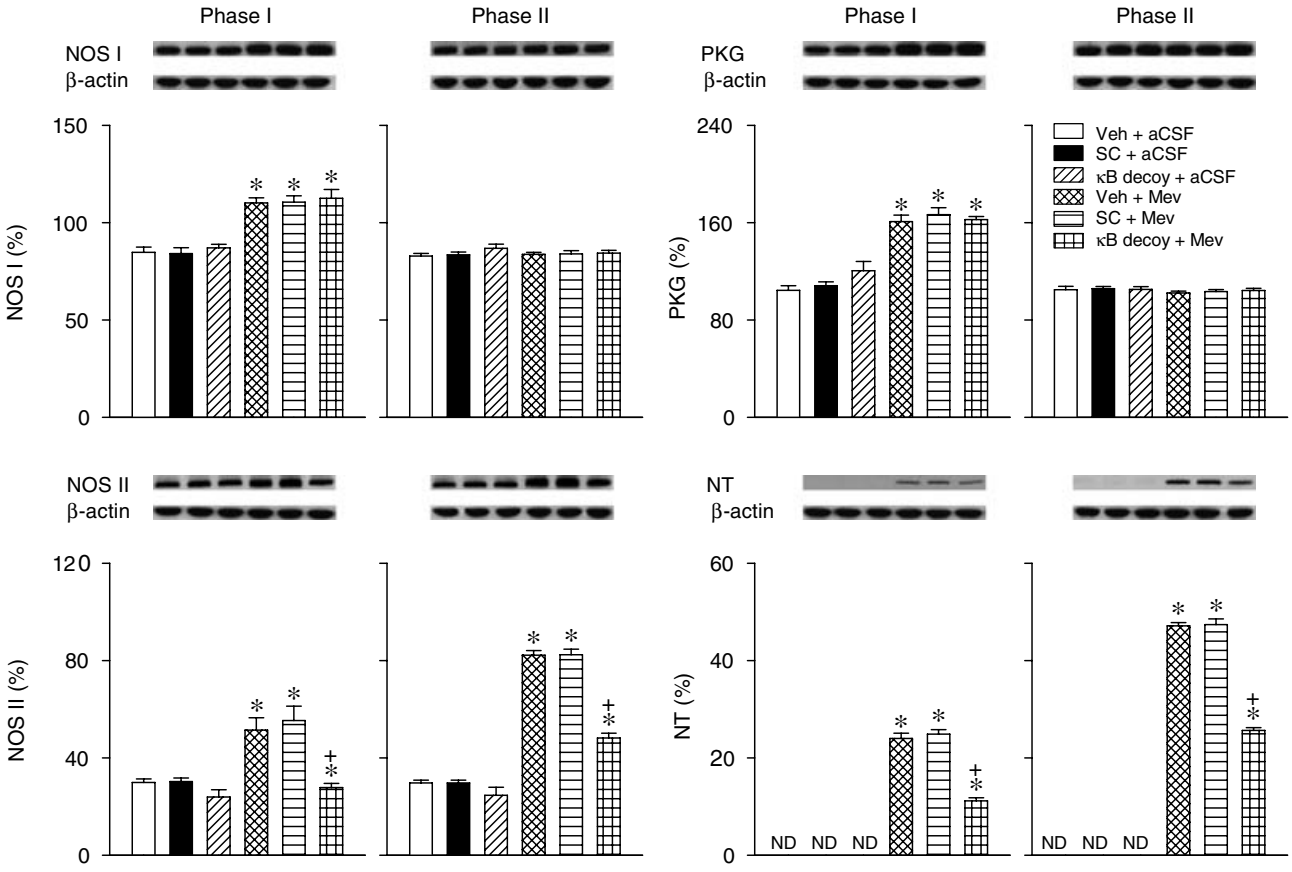

Figure 7. Effects of gene knockdown of NF-κB in RVLM on NOS I–PKG or NOS II–peroxynitrite signalling cascade in ventrolateral medulla during Mev intoxication
Representative Western blots (insets), or percentage of NOS I, II or III, PKG or NT relative to β-actin protein, detected from the ventrolateral medulla 30 min (Phase I) or 180 min (Phase II) after animals received bilateral microinjection into RVLM of Mev (10 nmol) or aCSF, given 24 h after pre-treatment with double-stranded κB decoy or scrambled (SC) DNA (100 pmol) or their solvent (Veh). Values are mean ± S.E.M. of triplicate analyses, $n = 5$–6 animals per experimental group. $^{*}P < 0.05$ *vs.* Veh + aCSF group, and $^{+}P < 0.05$ vs. Veh + Mev group in the Scheffé's multiple-range analysis. ND, below detection limit.

in the RVLM, in association with activation, respectively, of the sGC–cGMP–PKG cascade or peroxynitrite formation. This notion is supported by our observations that whereas the phasic changes in NOS I, PKG, NOS II or nitrotyrosine in ventrolateral medulla were antagonized by selective blockade of M2R or M4R, selective inhibition of M1R or M3R was ineffective. M2R immunoreactivity co-localizes with NOS I- or NOS II-immunoreactive cells in the RVLM (JYH Chan *et al.* 2004*a*). Furthermore, physiological regulation of sympathetic vasomotor outflow by the endogenous NO at the RVLM is concentration dependent and determined by a balance between the tonically active NOS I and NOS II (SHH Chan *et al.* 2001). A low concentration of NO generated by NOS I in the RVLM increases sympathetic vasomotor outflow (SHH Chan *et al.* 2001) by exciting sympathetic premotor neurons via a cGMP–PKG-dependent facilitation of presynaptic glutamate release (Huang *et al.* 2003). On the other hand, a high concentration of NO generated by NOS II decreases sympathetic vasomotor outflow (SHH Chan *et al.* 2001) by inhibiting RVLM neurons via a peroxynitrite-mediated reduction of presynaptic glutamate release (Huang *et al.* 2004).

Preferential transcriptional up-regulation of NOS II gene by NF-κB on activation of muscarinic M2R or M4R in RVLM underlies cardiovascular depression during the 'pro-death' phase of Mev intoxication

The 5′-flanking regulatory region of the human (Hall *et al.* 1994) or rabbit (Jeong *et al.* 2000) NOS I promoter contains NF-κB sequence of *cis*-acting DNA elements that may be responsible for its transcriptional regulation. NF-κB-binding sites are also present in the rat (Keinanen *et al.* 1999) or mouse (Wei *et al.* 2004) NOS II promoter, and are considered to be critical for gene expression. NF-κB is crucial for NOS I expression in the lumbar spinal cord of adult rats during the late stage of hyperalgesia (CF Chan *et al.* 2000), and for NOS II expression in human epithelial cells in response to pro-inflammatory cytokines and oxidants (Barnes, 1995). Thus, both NOS I (Hall *et al.* 1994; CF Chan *et al.* 2000; Jeong *et al.* 2000) and NOS II (Baeuerle & Henkel, 1994; Xie *et al.* 1994; Keinanen *et al.* 1999; Wei *et al.* 2004) genes are potentially regulated transcriptionally by NF-κB.

Because of its association with inhibitory κB (IκB) (Baeuerle & Henkel, 1994), NF-κB is normally sequestered in the cytoplasm in an inactive state. Activation of NF-κB requires phosphorylation of IκB by IκB kinase, leading to degradation of IκB and disruption of the NF-κB–IκB complex. The dissociated NF-κB subsequently translocates from the cytoplasm to the nucleus where this transcription factor binds to the κB promoter region of target genes, including NOS I (Hall *et al.* 1994; Jeong *et al.* 2000) and NOS II (Xie *et al.* 1994; Keinanen *et al.* 1999; Wei *et al.* 2004). Complementary results from EMSA and double immunofluorescence staining coupled with confocal microscopy in the present study demonstrated that the DNA binding activity of NF-κB in RVLM neurons was significantly augmented on muscarinic M2R or M4R activation, alongside nucleus-bound translocation of this transcription factor. That the major subunit activated in the RVLM, as revealed by super shift assay, is the p65–p50 heterodimer is consistent with reports (DeMeester *et al.* 2001; Yeh *et al.* 2002; JYH Chan *et al.* 2004*b*) that the p65–p50 complex is the predominant form of NF-κB in the central nervous system. More intriguingly, our present results provided the first *in vivo* demonstration of the functional significance of NF-κB activation, via preferential transcriptional up-regulation of the NOS II gene in the RVLM, in the manifestation of the 'pro-death' phase of Mev intoxication. Functional blockade of NF-κB binding to its cognate site, κB element by the double-stranded κB decoy DNA or by selective NF-κB antagonists in the RVLM significantly and preferentially blunted the Mev-induced surge in NOS II or peroxynitrite and the elicited reduction in low-frequency power and hypotension during phase II Mev intoxication. Our confocal images also indicated the presence of background NF-κB immunoreactivity in the RVLM. Since it was not double-labelled with NeuN, it is unlikely to be of neuronal origin. Transcriptional activation of NOS II via NF-κB has been reported in glial cells (Bhat *et al.* 2003). As NOS II is present in astrocytes and microglia at the RVLM (SHH Chan *et al.* 2005), it is conceivable that our observed preferential transcriptional up-regulation of NOS II gene by NF-κB in the manifestation of the 'pro-death' phase of Mev intoxication may also engage these glial cells in this medullary site. This notion, however, requires further elucidation.

Stimulation of muscarinic receptors leads to NF-κB activation (Todisco *et al.* 1999; Siehler *et al.* 2001). Of the very limited reports available, activation of NF-κB has been demonstrated in PC12 cells expressing cloned muscarinic M1R receptors (Mangelus *et al.* 2001), or in COS-7 cells expressing M3R (Yajeya *et al.* 2000). The present study provided the first demonstration that selective stimulation of native muscarinic M2R and M4R, but not M1R or M3R, in the RVLM resulted in NF-κB activation, leading to the augmented expression of NOS II that underlies the cardiovascular depression during phase II Mev intoxication. The interposing signalling pathways between stimulation of M2R or M4R and activation of NF-κB, as well as those that lead to up-regulation of NOS I gene, remain to be delineated.

Implications for brain stem death

In a series of systematically coordinated translational research (see JYH Chan *et al.* 2005*b* for review), our

laboratory has demonstrated that a common denominator exists among patients who succumbed to systemic inflammatory response syndrome (Yien *et al.* 1997), severe brain injury (Kuo *et al.* 1997*b*) or organophosphate poisoning (Yen *et al.* 2000). Death is invariably preceded by a dramatic reduction or loss of a 'life-and-death' signal that emanates from the RVLM (Kuo *et al.* 1997*a*) and manifests itself as the low-frequency component in the SAP spectrum (JYH Chan *et al.* 2005*b*). It follows that the distinct phases of augmentation ('pro-life') followed by reduction ('pro-death') of the low-frequency component in the SAP spectrum exhibited in our Mev intoxication model provide a succinct functional demonstration of the interplay between the central cardiovascular regulatory machinery at the RVLM and the progression towards brain stem death. The clinical relevance of this model is further reinforced by the observation that a common manifestation of patients who suffer from organophosphate poisoning, including Mev, is hypoxia resulting from respiratory depression (Yen *et al.* 2000). Intriguingly, Mev also induces mitochondrial dysfunction, bioenergetic failure and tissue hypoxia in the RVLM, leading to hypotension (Yen *et al.* 2005). As revealed by the augmented low-frequency power, which mirrors an enhanced BRR-mediated sympathetic vasomotor tone (Li *et al.* 2001), the maintained SAP during phase I Mev intoxication reflects effective central cardiovascular machinery against this elicited hypotension. During phase II, the progressive decrease in SAP becomes significant on reduction in the power density of the low-frequency component to below baseline.

With the realization that NO derived from NOS I and NOS II in the RVLM plays, respectively, a key role in the 'pro-life' and 'pro-death' phase in our Mev intoxication model of brain stem death (JYH Chan *et al.* 2004*a*, 2005*a*,*b*, 2007), it is crucial that the intracellular signalling cascades linking stimulation of muscarinic receptors to activation of these two NOS isoforms must be identified. The present study provided novel information in this direction by showing that selective stimulation of muscarinic M2R or M4R in the RVLM results in activation of NF-κB and both NOS I–PKG and NOS II–peroxynitrite cascades in the ventrolateral medulla, leading to both 'pro-life' and 'pro-death' phases of cardiovascular responses during Mev intoxication. Intriguingly, we further unveiled that this muscarinic activation of NF-κB is involved preferentially in eliciting cardiovascular depression during the 'pro-death' phase via transcriptional up-regulation of the NOS II gene in the RVLM in our Mev intoxication model of brain stem death. This information should provide further insights on the deterioration of central cardiovascular regulation during the progression towards brain stem death, and offer new vistas in devising therapeutic strategy or clinical management against this fatal eventuality.

References

Arneric SP, Giuliano R, Ernsberger P, Underwood MD & Reis DJ (1990). Synthesis, release and receptor binding of acetylcholine in the C1 area of the rostral ventrolateral medulla: contributions in regulating arterial pressure. *Brain Res* **511**, 98–112.

Baeuerle PA & Henkel T (1994). Function and activation of NF-κB in the immune system. *Annu Rev Immunol* **12**, 141–179.

Barnes PJ (1995). Nitric oxide and airway disease. *Ann Med* **27**, 389–393.

Bhat NR, Shen Q & Fan F (2003). TAK1-mediated induction of nitric oxide synthase gene expression in glial cells. *J Neurochem* **87**, 238–247.

Chan CF, Sun WZ, Lin JK & Lin-Shiau SY (2000). Activation of transcription factors of nuclear factor κB, activator protein-1 and octamer factors in hyperalgesia. *Eur J Pharmacol* **402**, 61–68.

Chan JYH, Chan SHH & Chang AYW (2004*a*). Differential contributions of NOS isoforms in the rostral ventrolateral medulla to cardiovascular responses associated with mevinphos intoxication in the rat. *Neuropharmacology* **46**, 1184–1194.

Chan JYH, Chan SHH, Li FCH, Cheng HL & Chang AYW (2005*a*). Phasic cardiovascular responses to mevinphos are mediated through differential activation of cGMP/PKG cascade and peroxynitrite via nitric oxide generated in the rat rostral ventrolateral medulla by NOS I and II isoforms. *Neuropharmacology* **48**, 161–172.

Chan JYH, Chang AYW & Chan SHH (2005*b*). New insights on brain stem death: From bedside to bench. *Prog Neurobiol* **77**, 396–425.

Chan JYH, Cheng HL, Chou JLJ, Li FCH, Dai KY, Chan SHH & Chang AYW (2007). Heat shock protein 60 or 70 activates NOS 1- and inhibits NOS II-associated signaling, and depresses mitochondrial apoptotic cascade during brain stem death. *J Biol Chem* **282**, 4585–4600.

Chan JYH, Ou CC, Wang LL & Chan SHH (2004*b*). Heat shock protein 70 confers cardiovascular protection during endotoxemia via inhibition of nuclear factor-κB activation and inducible nitric oxide synthase expression in rostral ventrolateral medulla. *Circulation* **110**, 3560–3566.

Chan SHH, Wang LL, Wang SH & Chan JYH (2001). Differential cardiovascular responses to blockade of nNOS or iNOS in rostral ventrolateral medulla of the rat. *Br J Pharmacol* **133**, 606–614.

Chan SHH, Wu KLH, Wang LL & Chan JYH (2005). Nitric oxide- and superoxide-dependent mitochondrial signaling in endotoxin-induced apoptosis in the rostral ventrolateral medulla of rats. *Free Radic Biol Med* **39**, 603–618.

Chang AYW, Chan JYH & Chan SHH (2003). Differential distribution of nitric oxide synthase isoforms in rostral ventrolateral medulla of the rat. *J Biomed Sci* **10**, 285–291.

Chang AYW, Chan JYH, Chou JLJ, Li FCH, Dai KY & Chan SHH (2006). Heat shock protein 60 in rostral ventrolateral medulla reduces cardiovascular fatality during endotoxemia in the rat. *J Physiol* **574**, 547–564.

DeMeester SL, Buchman TG & Cobb FP (2001). The heat shock paradox: NF-κB determine cell fate? *FASEB J* **15**, 270–274.

Ernsberger P, Arango V & Reis DJ (1988). A high density of muscarinic receptors in the rostral ventrolateral medulla is revealed by correction for autoradiographic efficiency. *Neurosci Lett* **85**, 179–186.

Giraldo E, Micheletti R, Montagna E, Giachetti A, Vigano MA, Ladinsky H & Melchiorre C (1988). Binding and functional characterization of the cardioselective muscarinic antagonist methoctramine. *J Pharmacol Exp Ther* **244**, 1016–1020.

Guertzenstein PG & Silver A (1974). Fall in blood pressure produced from discrete regions of the ventral surface of the medulla by glycine and lesions. *J Physiol* **242**, 489–503.

Hagan JJ, Jansen JH & Broekkamp CL (1987). Blockade of spatial learning by the M1 muscarinic antagonist pirenzepine. *Psychopharmacology* **93**, 470–476.

Hall AV, Antoniou H, Wang Y, Cheung AH, Arbus AM, Olson SL, Lu WC, Kau CL & Marsden PA (1994). Structural organization of the human neuronal nitric oxide synthase gene (NOS1). *J Biol Chem* **269**, 33082–33090.

Hill WD, Hess DC, Carroll JE, Wakade CG, Howard EF, Chen Q, Cheng C, Martin-Studdard A, Waller JL & Beswick RA (2001). The NF-κB inhibitor diethyldithiocarbamate (DDTC) increases brain cell death in a transient middle cerebral artery occlusion model of ischemia. *Brain Res Bull* **55**, 375–386.

Huang CC, Chan SHH & Hsu KS (2003). cGMP/protein kinase G-dependent potentiation of glutamatergic transmission induced by nitric oxide in immature rat rostral ventrolateral medulla neurons *in vitro*. *Mol Pharmacol* **64**, 521–532.

Huang CC, Chan SHH & Hsu KS (2004). 3-Morpholinylsydnonimine inhibits glutamatergic transmission in rat rostral ventrolateral medulla via peroxynitrite formation and adenosine release. *Mol Pharmacol* **66**, 492–501.

Huangfu D, Schreihofer AM & Guyenet PG (1997). Effect of cholinergic agonists on bulbospinal C1 neurons in rats. *Am J Physiol* **272**, R249–R258.

Jeong Y, Won J, Kim C & Yim J (2000). 5′-Flanking sequence and promoter activity of the rabbit neuronal nitric oxide synthase (nNOS) gene. *Mol Cell* **10**, 566–574.

Keinanen R, Vartiainen N & Koistinaho J (1999). Molecular cloning and characterization of the rat inducible nitric oxide synthase (iNOS) gene. *Gene* **234**, 297–305.

Kellar KJ, Martino AM, Hall DP Jr, Schwartz RD & Taylor RL (1985). High-affinity binding of [^{3}H]acetylcholine to muscarinic cholinergic receptors. *J Neurosci* **5**, 1577–1582.

Kobayashi RM, Brownstein M, Saavedra JM & Palkovits M (1975). Choline acetyltransferase content in discrete regions of the rat brain stem. *J Neurochem* **24**, 637–640.

Kubo T, Taguchi K, Sawai N, Ozaki S & Hagiwara Y (1997). Cholinergic mechanisms responsible for blood pressure regulation on sympathoexcitatory neurons in the rostral ventrolateral medulla of the rat. *Brain Res Bull* **42**, 199–204.

Kuo TBJ, Yang CCH & Chan SHH (1997*a*). Selective activation of vasomotor component of SAP spectrum by nucleus reticularis ventrolateralis in rats. *Am J Physiol* **272**, H485–H492.

Kuo TBJ, Yien HW, Hseu SS, Yang CCH, Lin YY, Lee LC & Chan SHH (1997*b*). Diminished vasomotor component of systemic arterial pressure signals and baroreflex in brain death. *Am J Physiol* **273**, H1291–H1298.

Li FCH, Chan JYH, Chan SHH & Chang AYW (2005). In the rostral ventrolateral medulla, the 70 kDa heat shock protein (HSP70), but not HSP90, confers neuroprotection against fatal endotoxemia via augmentation of nitric oxide synthase I (NOS I)/protein kinase G signaling pathway and inhibition of NOS II/peroxynitrite cascade. *Mol Pharmacol* **68**, 179–192.

Li P, Zhu DN, Kao KM, Lin Q & Sun SY (1995). Role of acetylcholine, corticoids and opioids in the rostral ventrolateral medulla in stress-induced hypertensive rats. *Biol Signals* **4**, 124–132.

Li PL, Chao YM, Chan SHH & Chan JYH (2001). Potentiation of baroreceptor reflex response by heat shock protein 70 in nucleus tractus solitarii confers cardiovascular protection during heatstroke. *Circulation* **103**, 2114–2119.

Liu J & Lee TJ (1999). Mechanism of prejunctional muscarinic receptor-mediated inhibition of neurogenic vasodilation in cerebral arteries. *Am J Physiol* **276**, H194–H204.

Mangelus M, Kroyter A, Galron R & Sokolovsky M (2001). Reactive oxygen species regulate signaling pathways induced by M1 muscarinic receptors in PC12M1 cells. *J Neurochem* **76**, 1701–1711.

Milner TA, Pickel VM, Giuliano R & Reis DJ (1990). Ultrastructural localization of choline acetyltransferase in the rat rostral ventrolateral medulla: evidence for major synaptic relations with non-catecholaminergic neurons. *Brain Res* **500**, 67–89.

Palkovits M & Jacobowitz DM (1974). Topographic atlas of catecholamine and acetylcholinesterase-containing neurons in the rat brain. II. Hindbrain (mesencephalon, rhombencephalon). *J Comp Neurol* **157**, 29–42.

Pallis C (1983). *A B C of Brain Stem Death*. British Medical Journal Press, London.

Paxinos G & Watson C (2007). *The Rat Brain in Stereotaxic Coordinates*, 6th edn. Academic Press, London.

Ross CA, Ruggiero DA, Park DH, Joh TH, Sved AF, Fernandez-Pardal J, Saavedra JM & Reis DJ (1984). Tonic vasomotor control by the rostral ventrolateral medulla: effect of electrical or chemical stimulation of the area containing C_1 adrenaline neurons on arterial pressure, heart rate, and plasma catecholamines and vasopressin. *J Neurosci* **4**, 474–494.

Schreck R, Meier B, Männel DN, Dröge W & Baeuerle PA (1992). Dithiocarbamates as potent inhibitors of nuclear factor κB activation in intact cells. *J Exp Med* **175**, 1181–1194.

Siehler S, Wang Y, Fan X, Windh RT & Manning DR (2001). Sphingosine 1-phosphate activates nuclear factor-κB through Edg receptors. Activation through Edg-3 and Edg-5, but not Edg-1, in human embryonic kidney 293 cells. *J Biol Chem* **276**, 48733–48739.

Spyer KM (1994). Central nervous mechanisms contributing to cardiovascular control. *J Physiol* **474**, 1–19.

Takahashi H, Kojima T, Ikeda T, Tsuda S & Shirasu Y (1991). Differences in the mode of lethality produced through intravenous and oral administration of organophosphorus insecticides in rats. *Fundm Appl Toxicol* **16**, 459–468.

Todisco A, Ramamoorthy S, Pausawasdi N & Tacey K (1999). Carbachol activates IκB kinase in isolated canine gastric parietal cells. *Biochem Biophys Res Comm* **261**, 877–884.

Waelbroeck M, Camus J, Tastenoy M & Christophe J (1992). Binding properties of nine 4-diphenyl-acetoxy-N-methyl-piperidine (4-DAMP) analogues to M1, M2, M3 and putative M4 muscarinic receptor subtypes. *Br J Pharmacol* **105**, 97–102.

Wei J, Guo H, Gao C & Kuo PC (2004). Peroxide-mediated chromatin remodelling of a nuclear factor κB site in the mouse inducible nitric oxide synthase promoter. *Biochem J* **377**, 809–818.

Willette RN, Punnen S, Krieger AJ & Sapru HN (1984). Cardiovascular control by cholinergic mechanisms in the rostral ventrolateral medulla. *J Pharmacol Exp Ther* **231**, 457–463.

Xie QW, Kahsiwabara Y & Nathan C (1994). Role of transcription factor NF-κB/Rel in induction of nitric oxide synthase. *J Biol Chem* **269**, 4705–4708.

Yajeya J, De La Fuente A, Criado JM, Bajo V, Sanchez-Riolobos A & Heredia M (2000). Muscarinic agonist carbachol depresses excitatory synaptic transmission in the rat basolateral amygdala in vitro. *Synapse* **38**, 151–160.

Yang CH, Shyr MH, Kuo TBJ, Tan PPC & Chan SHH (1995). Effects of propofol on nociceptive response and power spectra of electroencephalographic and systemic arterial pressure signals in the rat: correlation with plasma concentration. *J Pharmacol Exp Ther* **275**, 1568–1574.

Yeh SH, Lin CH, Lee CF & Gean PW (2002). A requirement of nuclear factor-κB activation in fear-potentiated startle. *J Biol Chem* **277**, 46720–46729.

Yen DHT, Chan JYH, Huang CI, Lee CH, Chan SHH & Chang AYW (2005). Coenzyme Q10 confers cardiovascular protection against acute mevinphos intoxication by ameliorating bioenergetic failure and hypoxia in the rostral ventrolateral medulla of the rat. *Shock* **23**, 353–359.

Yen DHT, Yen JC, Len WB, Wang LM, Lee CH & Chan SHH (2001). Spectral changes in systemic arterial pressure signals during acute mevinphos intoxication in the rat. *Shock* **15**, 35–41.

Yen DHT, Yien HW, Wang LM, Lee CH & Chan SHH (2000). Spectral analysis of systemic arterial pressure and heart rate signals of patients with acute respiratory failure induced by severe organophosphate poisoning. *Crit Care Med* **28**, 2805–2811.

Yien HW, Hseu SS, Lee LC, Kuo TBJ, Lee TY & Chan SHH (1997). Spectral analysis of systemic arterial pressure and heart rate signals as a prognostic tool for the prediction of patient outcome in intensive care unit. *Crit Care Med* **25**, 258–266.

Acknowledgements

This study was supported by research grants NSC-95-2752-B-075B-001-PAE (J.Y.H.C) and NSC-95-2752-B-110-001-PAE and NSC-95-2752-B-110-002-PAE (S.H.H.C and A.Y.W.C) from the National Science Council. S.H.H.C. is National Chair Professor of Neuroscience appointed by the Ministry of Education, and Sun Yat-sen Research Chair Professor appointed by National Sun Yat-sen University, Taiwan, Republic of China.